IOP Publishing Journal of Physics D: Applied Physics
J. Phys. D: Appl. Phys. **54** (2021) 065502 (8pp) https://doi.org/10.1088/1361-6463/abbe4a

Numerical modeling of ignition enhancement by repetitive nanosecond discharge in a hydrogen/air mixture II: forced ignition

Yuan Wang[1,2], **Peng Guo**[2], **Haitao Chen**[1] **and Zheng Chen**[2]

[1] Institute of Applied Physics and Computational Mathematics, Beijing 100094, People's Republic of China
[2] SKLTCS, CAPT, BIC-ESAT, College of Engineering, Peking University, Beijing 100871, People's Republic of China

E-mail: cz@pku.edu.cn

Received 13 May 2020, revised 22 September 2020
Accepted for publication 5 October 2020
Published 19 November 2020

Abstract

Non-equilibrium plasma has promising applications in combustion enhancement. In this study, 1D simulations are conducted for the forced ignition process using non-equilibrium plasma generated by repetitively pulsed nanosecond discharge (NSD). The ignition kernel is induced by a discharge area with NSD and it develops and propagates in a static stoichiometric hydrogen/air mixture. The objective is to assess how the characteristics of NSD affect the ignition delay time and ignition kernel development during the forced ignition process. Similar to the homogeneous ignition considered in part I, the forced ignition process is found to be strongly affected by the pulse number, discharge frequency, discharge radius, total input energy, and input energy per pulse of NSD. For a fixed input energy per pulse, the ignition delay time decreases and the propagation speed of the initial ignition kernel increases with the pulse number, discharge frequency and discharge radius. However, for a fixed total input energy, the ignition delay time increases and the propagation speed of the initial ignition kernel decreases with the pulse number. Furthermore, it is found that the promotion of ignition kernel development and propagation in the forced ignition by NSD are mainly due to the kinetic effect rather than the thermal effect.

Keywords nanosecond discharge, forced ignition, ignition kernel, kinetic effect

(Some figures may appear in colour only in the online journal)

1. Introduction

Non-equilibrium plasma has promising applications in combustion enhancement [1–3]. As a way to produce the non-equilibrium plasma, repetitively pulsed nanosecond discharge (NSD) has a relatively high electron temperature caused by efficient energy deposition during the nanosecond discharge process [1, 4]. Besides, NSD with a kHz repetition rate creates volumetric non-equilibrium plasma with high voltage [5]. Therefore, NSD has been popularly used to achieve plasma assisted combustion. For example, NSD has promising applications in terms of ignition and combustion enhancement in high speed propulsion systems, such as scramjet engines [2], in which successful ignition and subsequently complete combustion are challenging, due to the very short residence time [6, 7].

As introduced in part I [8], in the literature there are many studies on ignition enhancement using NSD. However, most of the previous studies mentioned in part I [8] are on NSD assisted autoignition, which is only controlled by chemical

kinetics and there is no heat or mass transport. This work is a continuation of part I [8], and the purpose is to assess how the characteristics of NSD affect the forced ignition process.

Recently, different groups have conducted experimental or numerical studies on the forced ignition caused by NSD. For examples, Lin *et al* [9] conducted experiments on the forced ignition caused by multi-channel nanosecond discharge plasma and demonstrated that the multi-channel nanosecond discharge has the advantages in achieving successful ignition at low pressures compared to spark discharge. The experiments of Stepanyan *et al* [10] also showed that compared to conventional spark discharge, nanosecond spark discharge with less energy can produce larger excited gas volume and thus promote ignition kernel development. Lefkowitz and Ombrello [11] conducted forced ignition experiments caused by NSD with high discharge frequency and found that the pulse repetition frequency affects the ignition probability and minimum ignition power. Sharma *et al* [12] numerically assessed the effects of plasma characteristics on ignition and flame propagation, and they found that the ignition enhancement is mainly due to the generation of radicals and extension of high temperature region by NSD. Tholin *et al* [13] conducted 2D simulations for the ignition of a lean hydrogen/air mixture by nanosecond spark discharge and showed that both the thermal and chemical effects are important for the forced ignition process. In their 1D simulations, Han and Yamashita [14] investigated the effects of the strength of the reduced electric field and discharge duration on the ignition delay time of the plasma-assisted ignition. Casteka *et al* [15] conducted experiments and 3D simulations for the ignition by NSD. They found that the gas flow recirculation from fresh gases to the discharge center greatly reduces hot kernel temperature and thereby changes the topology of the hot kernel.

Most of the previous studies mentioned above mainly focused on the ignition kernel development induced by NSD. However, the effects of NSD characteristics on the forced ignition process are still not well known. The objective of this study is to assess how the pulse number, discharge frequency, discharge radius, total input energy, and input energy per pulse of NSD affect the ignition delay time and ignition kernel development during the forced ignition process in a static stoichiometric hydrogen/air mixture. Numerical simulations are conducted using the in-house codes ZDPlasKin-CHEMKIN and A-SURF. The chemical kinetics and transport during the ignition kernel development and propagation processes are considered in simulations. In what follows, the numerical model and methods are introduced in section 2. Then in section 3, the forced ignition process is studied and the effects of NSD characteristics on the ignition delay time and ignition kernel development are investigated. Finally, the conclusions are summarized in section 4.

2. Numerical model and methods

We consider the forced ignition process in a quiescent stoichiometric H_2/air mixture at atmospheric pressure and the elevated temperature of $T_0 = 800$ K. The elevated temperature of 800 K is chosen so that the ignition delay time for the 1D forced ignition can be compared with that for 0D homogeneous ignition in part I. The NSD process has a timescale in the order of nanoseconds, while the characteristic time for ignition kernel and flame propagation is in the order of microseconds. Therefore, as a first step to understand the forced ignition enhancement by NSD, the discharge process and ignition kernel development process are separated in the present simulations. Specifically, first, the discharge process is considered as the 0D homogeneous ignition studied in part I [8]. Then the temperature and species concentrations obtained in the discharge process are uniformly added to the discharge area for the 1D forced ignition. The same procedure was used by Han and Yamashita [14] and Filimonova *et al* [16].

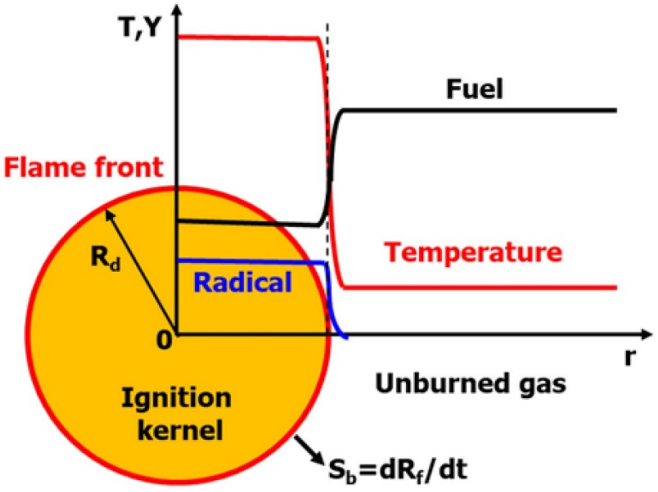

Figure 1. Schematic of the initial temperature and concentrations of fuel and radical in the 1D computational domain. The discharge area has the radius of R_d and the propagation speed of the ignition kernel is S_b.

The numerical setup is sketched in figure 1. Spherical symmetry is assumed and thereby 1D simulation is conducted. The spherical discharge area in the radius of R_d is located at the center. Compared to the surrounding mixture, the mixture inside the discharge area has a higher temperature and radical concentration due to NSD. The 1D computational domain is $0 \leqslant r \leqslant 10$ cm in a spherical coordinate. Initially, the mixture is static and the pressure in the whole domain is $P_0 = 1$ atm. At both boundaries, $r = 0$ and 10 cm, zero flow velocities and zero gradients of mass fractions and temperature are enforced.

As described in part I [8], the homogeneous ignition process is simulated using the in-house code ZDPlasKin-CHEMKIN [17], incorporating the plasma kinetics solver ZDPlasKin [18] and combustion kinetics solver CHEMKIN [19]. The Boltzmann equation solver, BOLSIG+ [20], is incorporated into ZDPlasKin to calculate the electron transport and reaction coefficients. This code is used to solve the temporal evolutions of species and temperature during the homogeneous ignition process. The details on equations for species and temperature and on code validation can be found in part I [8].

The spherical ignition kernel development and propagation processes are simulated using the in-house code A-SURF [21–23]. The conservation equations for unsteady, compressible, multi-component, reactive flow are solved using the finite volume method. The CHEMKIN packages are included to evaluate the chemical reaction rates, thermodynamic and transport properties. The Strang splitting fractional-step procedure is used to decouple hydrodynamic transport and stiff chemical reactions. In the first fractional step, the non-reactive flow is solved and the Runge-Kutta, MUSCL-Hancock and central difference schemes are used respectively for the temporal integration, convective fluxes and diffusive fluxes. In the second fractional step, the chemistry is solved using the VODE solver. Dynamically adaptive mesh refinement is employed and the ignition kernel or flame front is always fully covered by the finest mesh with a size of 4 μm. Numerical convergence is checked and ensured by further decreasing the time step and mesh size in simulation. A-SURF has been successfully used in previous studies on ignition and spherical flame propagation [24–27]. For example, the results in [28,29,] demonstrated that compared to experimental data, A-SURF can accurately predict the ignition and propagation of 1D spherical flames in mixtures initially at both normal and elevated temperatures. Details on governing equations, numerical schemes, and code validation of A-SURF can be found in [21–23] and thereby are not repeated here.

A kinetic model for H_2/air including both combustion and plasma chemistries is developed in part I [8] and it is used in the present simulation. The kinetic model consists of 20 species and 111 reactions. It incorporates neutral species H_2, O_2, H_2O, N_2, H_2O_2, O_3, H, O, OH and HO_2; charged species N_2^+, HN_2^+, H_3O^+, O_2^- and e; and excited species $N_2(A^3)$, $N_2(B^3)$, $N_2(C^3)$, $N_2(a^1)$ and $O(^1D)$. The combustion chemistry for H_2/air developed by Burke *et al* [30] is used. The plasma chemistry consists of plasma air kinetics and plasma hydrogen kinetics, in which the electron-collision cross sections for air and hydrogen are downloaded from the online database LXCat [31]. The reactions in plasma kinetic model of H2/air are listed in part I [8].

3. Results and discussion

As studied in part I [8], the electrical characteristics have great impact on the homogenous ignition of a stoichiometric H_2/air mixture using non-equilibrium plasma generated by NSD. Since the mixture in the discharge area for forced ignition is obtained from homogenous ignition with NSD, it is expected that the ignition kernel development and propagation are also affected by the electrical characteristics of the NSD. In the following, the effects of pulse number, n_p, discharge frequency, f, discharge radius, R_d, total input energy, E_0 and input energy per pulse, E_i, on the ignition delay time and ignition kernel propagation speed are investigated. It is noted that these variables are not independent in practical plasma-assisted combustion processes. For example, the input energy per pulse E_i can be affected by the reduced electric field E/N. In simulations, we make use of the advantage that these variables

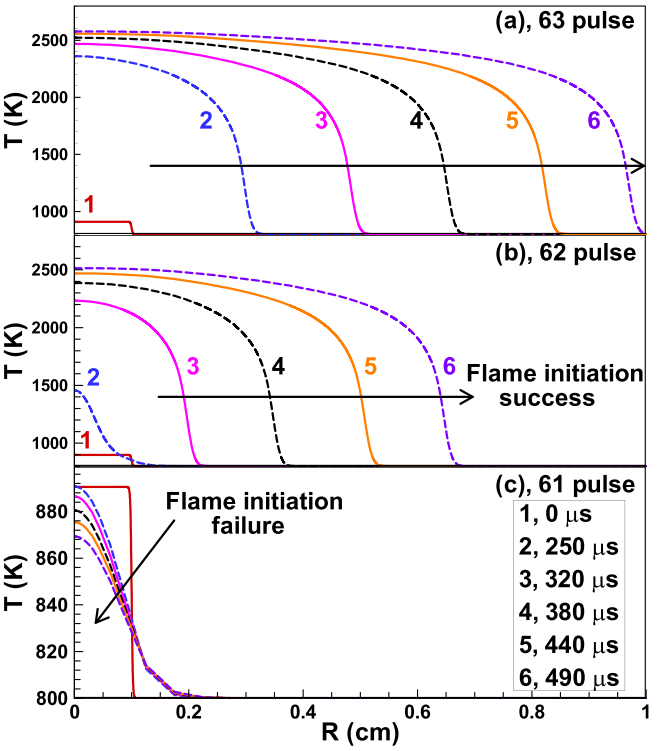

Figure 2. Temporal evolution of temperature distribution for fixed $E_i = 0.1$ mJ cm^{-3}, $f = 40$ kHz and $R_d = 1$ mm, but different values of pulse number: (a) $n_p = 63$, (b) $n_p = 62$ and (c) $n_p = 61$.

can be specified and changed independently. Consequently, the individual effect of each factor can be identified through changing only one variable and fixing other variables.

Figure 2 shows the temporal evolution of temperature distribution for fixed input energy per pulse of $E_i = 0.1$ mJ cm^{-3}, discharge frequency of $f = 40$ kHz and discharge radius of $R_d = 1$ mm, but different values of pulse number of $n_p = 61$, 62 and 63. It is seen that there is a critical pulse number, $n_{p,c} = 62$, below which the forced ignition fails and self-sustaining propagation of the spherical ignition kernel cannot be achieved. Specifically, after the 61st pulse (red line in figure 2(c)), the temperature reaches $T = 890.6$ K and then it gradually decreases for $R < R_d = 1$ mm and increases for $R > R_d = 1$ mm due to the heat conduction from the discharge area to the surrounding fresh mixture. When the pulse number is increased to $n_p = n_{p,c} = 62$, the forced ignition succeeds and ignition kernel propagates outwardly in a self-sustained manner as shown in figure 2(b). With further increase of the pulse number to $n_p = 63$, the ignition kernel propagates outwardly more rapidly. For the homogenous ignition process considered in part I [8], the critical pulse number for successful ignition is $n_{p,c} = 57$, which is smaller than the value of $n_{p,c} = 62$ for the forced ignition process. This is reasonable since there is heat and radical loss from the ignition kernel to the surrounding mixture during the forced ignition process. The temperature at the surface of $R_d = 1$ mm decreases from $T = 890.6$ K at $t = 0$ to $T = 834$ K at $t = 250$ μs (line 2 in figure 2(c)), which is lower than $T = 872$ K for $n_p = n_{p,c} = 57$ as shown in figure 3 of part I [8] and thereby the ignition fails. Comparison between

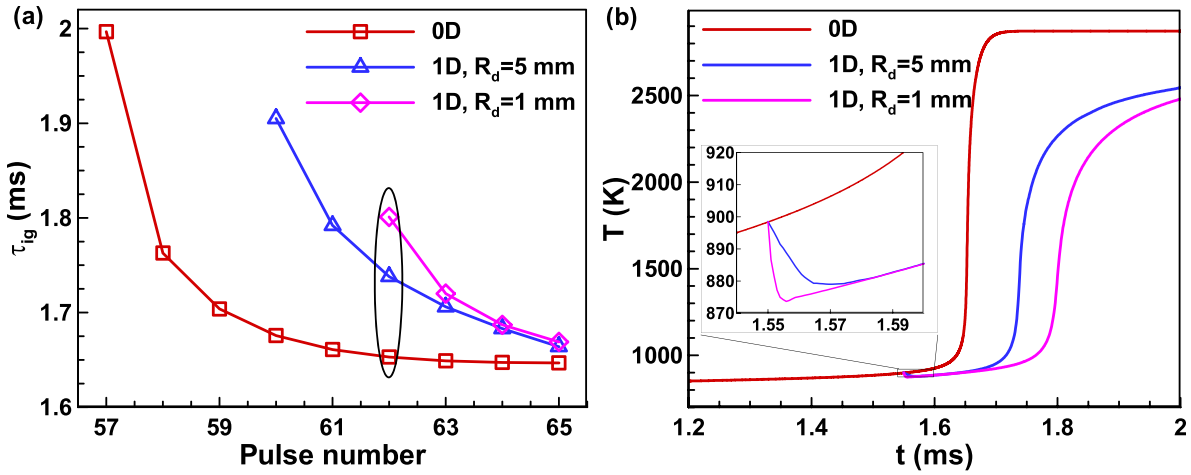

Figure 3. (a) Change of ignition delay time with pulse number and (b) the evolution of temperature for $n_p = 62$. The input energy per pulse of $E_i = 0.1$ mJ cm^{-3} and discharge frequency of $f = 40$ kHz are fixed but different values of discharge radius of $R_d = \infty$ (i.e. 0D homogeneous ignition), 5 and 1 mm are considered.

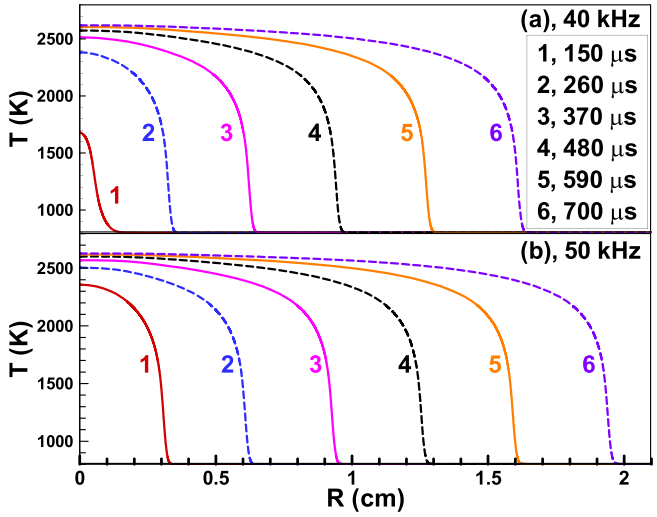

Figure 4. Temporal evolution of temperature distribution for fixed $E_i = 0.1$ mJ cm^{-3}, $n_p = 61$ and $R_d = 1$ mm, but different values of discharge frequency of $f = 40$ and 50 kHz.

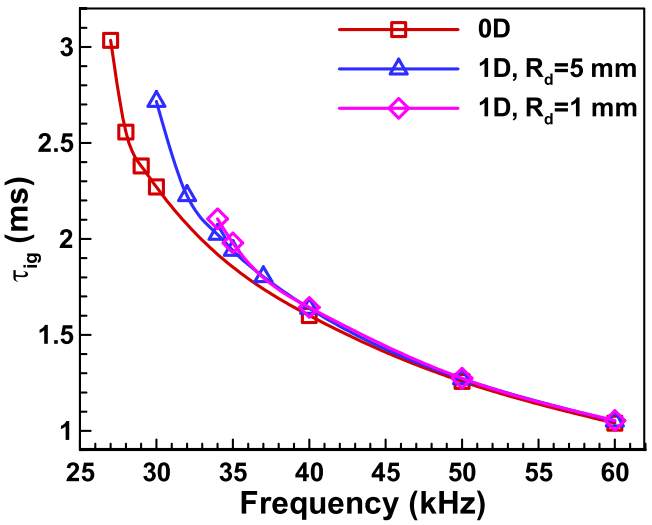

Figure 5. Change of ignition delay time with discharge frequency for fixed $E_i = 0.1$ mJ cm^{-3} and $n_p = 63$, but different values of discharge radius of $R_d = \infty$ (i.e. 0D homogeneous ignition), 5 and 1 mm.

figures 2(a) and (b) indicates that increasing pulse number can promote ignition kernel development and accelerate flame kernel propagation.

To assess the effects of pulse number and the size of discharge area on the forced ignition process, in figure 3(a) we plot the change of ignition delay time with a pulse number for fixed values of $E_i = 0.1$ mJ cm^{-3} and $f = 40$ kHz, but different values of $R_d = \infty$, 5 and 1 mm. The case of $R_d = \infty$ is equivalent to the 0D homogeneous ignition. The ignition delay time for the force ignition process is defined as the time when the maximum temperature reaches 1200 K (i.e. 400 K above the initial temperature $T_0 = 800$ K). For each given discharge radius, the ignition delay time decreases monotonically as the pulse number increases and it eventually approaches a constant value. For each given pulse number, a longer ignition delay time is observed for a smaller discharge radius since there is a smaller amount of heat and radical within the discharge zone. Besides, decreasing the discharge radius results in the increase of the critical pulse number. We have $n_{p,c} = 57$, 60 and 62 respectively for $R_d = \infty$, 5 and 1 mm. The evolution of temperature for a fixed pulse number of $n_p = 62$ but different values of discharge radius are compared in figure 3(b). After the 62nd pulse ($t = 1.55$ ms), the temperature reaches $T = 895$ K (see the insert in figure 3(b)). For the homogeneous ignition process, the temperature continuously increases and successful ignition occurs around $t = 1.65$ ms. For the forced ignition process, the temperature within the ignition kernel rapidly decreases due to the heat transport to the surrounding mixture. The temperature reaches the minimum value of 873 K at $t = 1.56$ ms for $R_d = 1$ mm and 879 K at $t = 1.57$ ms for $R_d = 5$ mm. Therefore, increasing the pulse number and

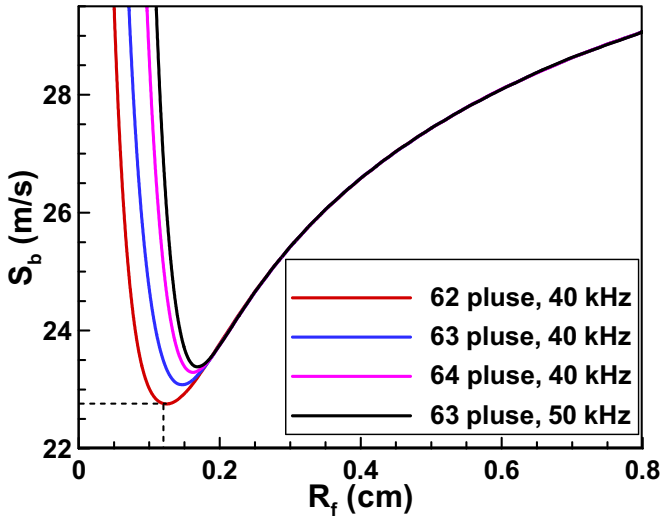

Figure 6. Change of flame propagation speed with flame radius for fixed $E_i = 0.1$ mJ cm^{-3} and $R_d = 1$ mm, but different values of pulse number of $n_p = 62$, 63 and 64, and discharge frequency of $f = 40$ and 50 kHz.

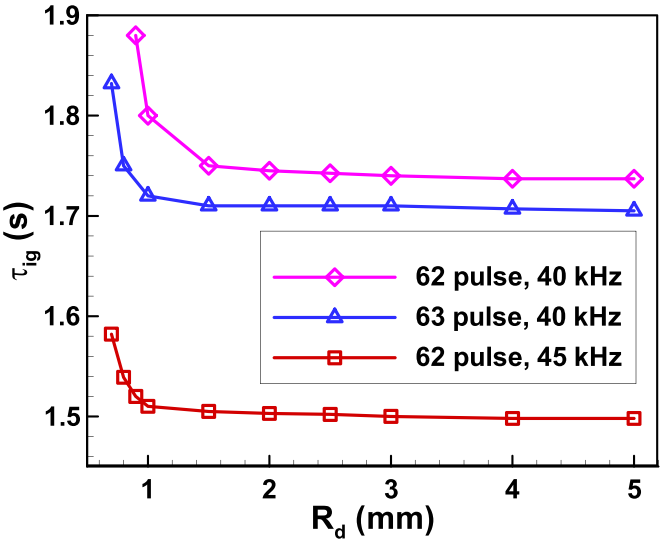

Figure 8. Change of ignition delay time with discharge radius for fixed $E_i = 0.1$ mJ cm^{-3}, but different values of pulse number of $n_p = 62$ and 63, and discharge frequency of $f = 40$ and 45 kHz.

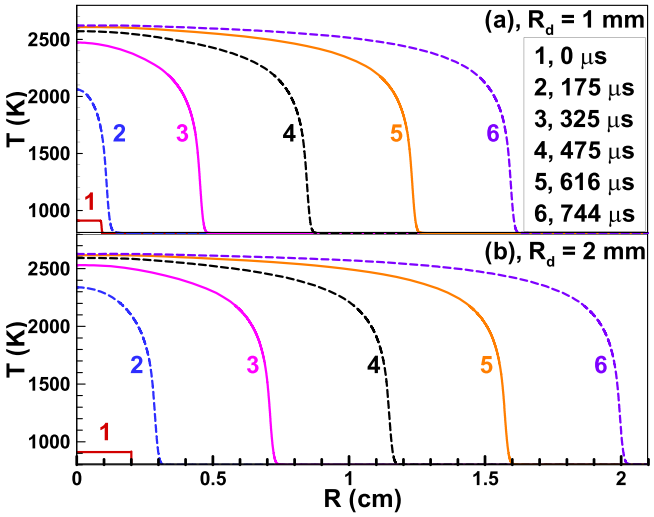

Figure 7. Temporal evolution of temperature distribution for fixed $E_i = 0.1$ mJ cm^{-3}, $n_p = 61$ and $f = 40$ kHz, but different values of discharge radius of $R_d = 1$ and 2 mm.

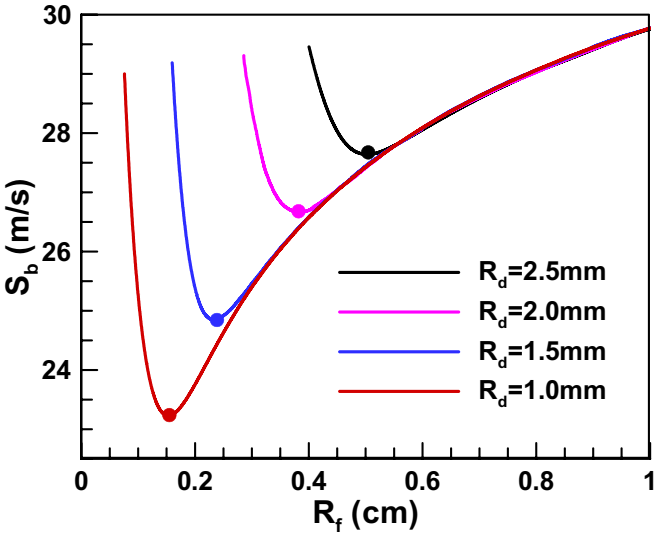

Figure 9. Change of flame propagation speed with flame radius for fixed $E_i = 0.1$ mJ cm^{-3}, $f = 40$ kHz and $n_p = 63$, but different values of discharge radius of $R_d = 1$, 1.5, 2 and 2.5 mm.

discharge radius can reduce ignition delay time and promote ignition. It is noted that the total input energy increases linearly with the pulse number and cubically with the discharge radius when the input energy per pulse is fixed.

Figure 4 shows the effect of discharge frequency on ignition kernel propagation. As with the discussion in part I [8], more radical accumulates between two consecutive discharges for the higher discharge frequency, resulting in higher temperature rise. In figure 4, the temperature at the center reaches $T = 1676$ K for $f = 40$ kHz and $T = 2356$ K for $f = 50$ kHz at $t = 150$ μs. Consequently, the ignition kernel with higher temperature and radical concentration readily develops and propagates outwardly at a higher speed is observed for $f = 50$ kHz.

The effects of discharge frequency and the size of discharge area on the ignition delay time of the force ignition process are demonstrated in figure 5. The ignition delay time is shown to decrease rapidly as the discharge frequency increases. Moreover, for discharge frequency above 40 kHz, the discharge radius has little influence on the ignition delay time, indicating that the heat and radical transport from the ignition kernel to the surrounding mixture do not affect the thermal runaway at the center. The results in figures 4 and 5 indicate that increasing discharge frequency can reduce the ignition delay time and accelerate the ignition kernel development and propagation.

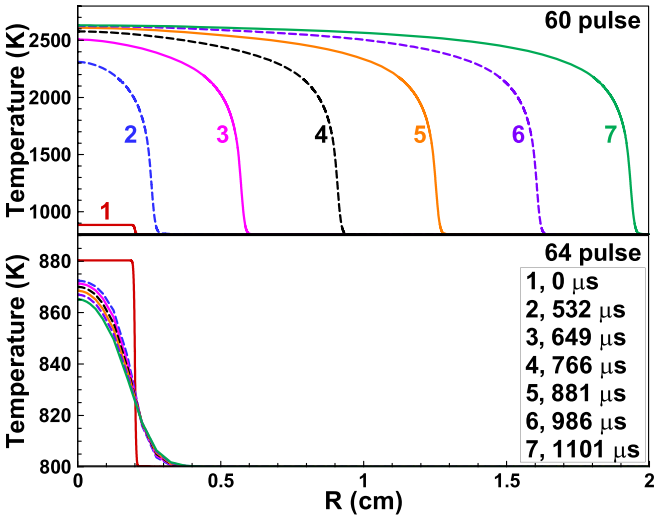

Figure 10. Temporal evolution of temperature distribution for fixed $E_0 = 6$ mJ cm^{-3}, $f = 40$ kHz and $R_d = 2$ mm, but different values of pulse number of $n_p = 60$ and 64.

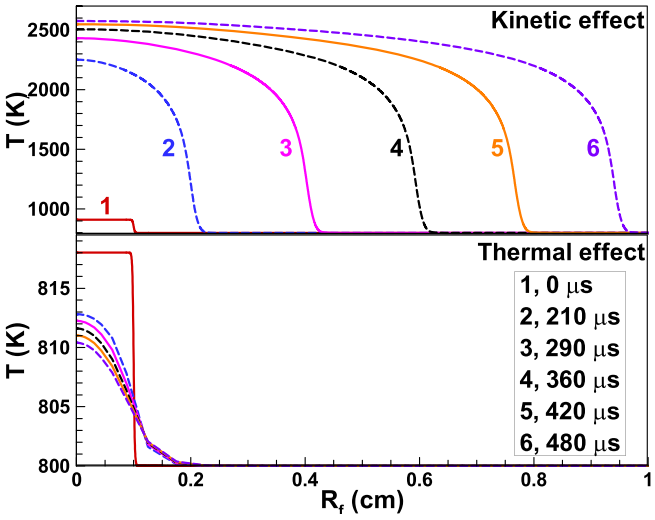

Figure 12. Temporal evolution of temperature distribution for fixed $E_i = 0.1$ mJ cm^{-3}, $f = 40$ kHz, $n_p = 63$ and $R_d = 1$ mm, but different total input energy modes.

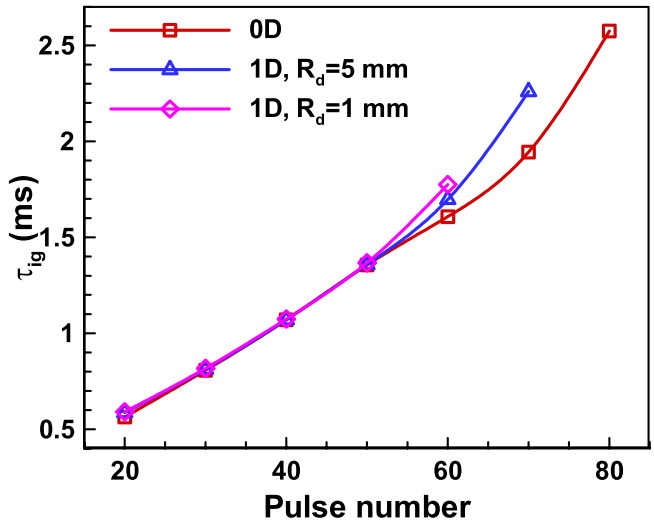

Figure 11. Change of ignition delay time with pulse number for fixed $E_0 = 6$ mJ cm^{-3} and $f = 40$ kHz, but different values of discharge radius of $R_d = \infty$ (i.e. 0D homogeneous ignition), 5 and 1 mm.

To assess the effects of pulse number and discharge frequency on ignition kernel propagation, in figure 6 we plot the flame propagation speed, S_b, as a function of the flame radius, R_f. In simulation, the flame radius is defined as the position of maximum heat release rate; and the flame propagation speed is calculated by $S_b = dR_f/dt$. The ignition kernel is shown to first decelerate and its propagation speed reaches the minimum value at some critical radius [23, 25, 32, 33]. The critical radius is $R_f = 0.12$ cm for $n_p = 62$ and $f = 40$ kHz. Successful ignition is achieved only when the ignition kernel can reach and propagate beyond this critical flame radius [23]. With the increase in the pulse number or discharge frequency, both the critical flame radius and the corresponding minimum flame propagation speed increase. Above the critical flame radius, the flame propagation speed is shown to increase monotonically with the flame radius. Furthermore, for $R_f > 0.2$ cm, the flame propagation speeds are independent of the pulse number and discharge frequency. Therefore, both the pulse number and discharge frequency affect the initial ignition kernel propagation while they have little influence on the quasi-steady propagation process.

The results in figures 3 and 5 indicate that the discharge radius affects the forced ignition process. To further assess the influence of discharge radius on ignition and the resulting ignition kernel development and propagation, we compare the results from different discharge radii in figures 7–9. Figure 7 compares the temporal evolution of temperature distribution for $R_d = 1$ and 2 mm. Since the input energy from NSD is proportional to the cube of the discharge radius, double the discharge radius results in much higher ignition energy and faster ignition kernel propagation.

Figure 8 summarizes the ignition delay time for a fixed input energy per pulse of $E_i = 0.1$ mJ cm^{-3}, but different values of discharge radius, pulse number, and discharge frequency. As the discharge radius increases, the ignition delay time is shown to decrease rapidly for $R_d < 1.5$ mm and it approaches a nearly constant value for $R_d \geqslant 1.5$ mm. This indicates that there is an optimum discharge radius, beyond which further enhancement of the forced ignition cannot be achieved at the cost of increasing the ignition energy from NSD. Besides, figure 8 shows that increasing the pulse number or discharge frequency can efficiently reduce the ignition delay time and thereby promote ignition kernel development and propagation.

Figure 9 shows the effects of discharge radius on the propagation speed of the initial ignition kernel. Successful ignition is achieved for these four discharge radii. The critical flame initiation radius is shown to increase with the discharge radius. Moreover, similar to the results in figure 6, above the

critical flame initiation radius, the different flame propagation speed trajectories converge onto a single curve, indicating that the NSD only affects the initial ignition kernel propagation while it has little influence beyond the critical flame radius.

The above results are for a fixed input energy per pulse, E_i, and thereby the total input energy, E_0, is proportional to the pulse number, n_p. In the following, we assess the effect of input energy per pulse on the forced ignition process for a fixed total input energy. Figure 10 shows the temporal evolution of temperature distribution for a fixed total input energy of $E_0 = 6$ mJ cm^{-3}, discharge frequency of $f = 40$ kHz and discharge radius of $R_d = 2$ mm, but different pulse numbers of $n_p = 60$ and 64. The input energy per pulse is $E_i = 0.1$ mJ cm^{-3} for $n_p = 60$ and $E_i = 0.09375$ mJ cm^{-3} for $n_p = 64$. Successful ignition is observed for $n_p = 60$ while ignition fails for $n_p = 64$. As shown in figure 7 of part I [8] for the homogenous ignition process, the ignition delay time increases with the pulse number when the total input energy is fixed. In the forced ignition process, the longer ignition delay time results in a larger amount of heat and radical loss, due to transportation from the ignition kernel to the surrounding mixture, and thereby causes ignition failure for the larger pulse number of $n_p = 64$. Therefore, the forced ignition process is affected by not only the total input energy E_0 but also the input energy per pulse E_i, which is equal to E_0/n_p.

Figure 11 demonstrates the effects of pulse number on the ignition delay time for fixed total input energy of $E_0 = 6$ mJ cm^{-3} and discharge frequency of $f = 40$ kHz, but different discharge radii of $R_d = \infty$, 5 and 1 mm. The ignition delay time increases monotonically with the pulse number for each discharge radius. For $n_p < 50$, the ignition delay time is independent of the discharge radius. This is because the heat and radical transport from the ignition kernel to the surrounding mixture do not affect the thermal runaway at the center. For $n_p > 50$, the ignition delay time is shown to become longer for smaller discharge radii, which have a larger amount of heat and radical loss transported to the mixture surrounding the ignition kernel. Therefore, figures 3(a) and 11 demonstrate that both the total input energy and input energy per pulse can affect the ignition delay time for the forced ignition process.

For the homogeneous ignition process studied in part I [8], the ignition enhancement by NSD is mainly due to the kinetic effects while the thermal effects (Joule heat) are negligible. Similarly, we compare the kinetic and thermal effects of NSD on the forced ignition process in figure 12. The total energy from NSD mainly contributes to the production of Joule heat (referred to as the thermal effect) and excited species and radicals (referred to as the kinetic effect) [4, 8]. To separately assess the thermal and kinetic effects involved in the forced ignition process, we conduct the simulations considering only the kinetic or thermal effect. Figure 12 shows that successful ignition is achieved for the case only considering the kinetic effect, while ignition fails for the case only considering thermal effect. This indicates that for the forced ignition caused by NSD, the kinetic effect dominates over the thermal effect.

4. Conclusions

The forced ignition by NSD in a stoichiometric hydrogen/air mixture is simplified in simulations by separating the 0D discharge process and 1D ignition kernel development process. The effects of NSD characteristics on the ignition delay time and ignition kernel propagation during the forced ignition are examined. It is found that for a fixed input energy per pulse, increasing the pulse number, discharge frequency, and/or discharge radius can reduce the ignition delay time and accelerate the initial ignition kernel propagation. This is because the total input energy becomes higher for larger pulse number and/or discharge radius, and more radical accumulates at higher discharge frequency. There is an optimum discharge radius, beyond which further enhancement of the forced ignition cannot be achieved at the cost of increasing the ignition energy from NSD. The ignition delay time and ignition kernel propagation speed are affected by not only the total input energy but also the input energy per pulse. For a fixed total input energy, the ignition delay time increases monotonically with the pulse number. Furthermore, the promotion of ignition kernel development and propagation in forced ignition by NSD is mainly due to the kinetic effect rather than the thermal effect.

It is noted that this work is a first step towards a better understanding of the influence of NSD on the forced ignition, which is simplified as two separated processes. In future works, it would be interesting to couple the discharge and ignition kernel development processes. Moreover, the 1D symmetry is assumed and a static mixture is considered here. The multi-dimensional effects and flow effects need to be explored in future studies.

Acknowledgments

This work was supported by the National Natural Science Foundation of China (Nos. 51861135309 and 91741126).

ORCID iDs

Yuan Wang https://orcid.org/0000-0001-5597-066X
Zheng Chen https://orcid.org/0000-0001-7341-6099

References

[1] Ju Y and Sun W 2015 Plasma assisted combustion: dynamics and chemistry *Prog. Energy Combust. Sci.* **48** 21–83
[2] Ju Y and Sun W 2015 Plasma assisted combustion: progress, challenges, and opportunities *Combust. Flame* **162** 529–32
[3] Sun W and Ju Y 2013 Nonequilibrium plasma-assisted combustion: a review of recent progress *J. Plasma Fusion Res.* **89** 208–19
[4] Lefkowitz J K, Guo P, Ombrello T, Won S H, Stevens C A, Hoke J L, Schauer F and Ju Y 2015 Schlieren imaging and pulsed detonation engine testing of ignition by a nanosecond repetitively pulsed discharge *Combust. Flame* **162** 2496–507

[5] Nagaraja S, Yang V, Yin Z and Adamovich I 2014 Ignition of hydrogen-air mixtures using pulsed nanosecond dielectric barrier plasma discharges in plane-to-plane geometry *Combust. Flame* **161** 1026–37
[6] Ombrello T, Ju Y and Fridman A 2008 Kinetic ignition enhancement of diffusion flames by nonequilibrium magnetic gliding arc plasma *AIAA J.* **46** 2424–33
[7] Ombrello T and Ju Y 2008 Kinetic ignition enhancement of H_2 versus fuel-blended air diffusion flames using nonequilibrium plasma *IEEE Trans. Plasma Sci.* **36** 2924–32
[8] Wang Y, Guo P, Chen H and Chen Z 2020 Numerical modeling of ignition enhancement by nanosecond repetitively pulsed discharge in a hydrogen/air mixture I: calculations assuming homogenous ignition *J. Phys. D: Appl. Phys.* **54** 065501
[9] Lin B X, Wu Y, Zhang Z B and Chen Z 2017 Multi-channel nanosecond discharge plasma ignition of premixed propane/air under normal and sub-atmospheric pressures *Combust. Flame* **182** 102–13
[10] Stepanyan S, Minesi N, Tibère-Inglesse A, Salmon A, Stancu G D and Laux C O 2019 Spatial evolution of the plasma kernel produced by nanosecond discharges in air *J. Phys. D: Appl. Phys.* **52** 295203
[11] Lefkowitz J K and Ombrello T 2017 An exploration of inter-pulse coupling in nanosecond pulsed high frequency discharge ignition *Combust. Flame* **180** 136–47
[12] Sharma A, Subramaniam V, Solmaz E and Raja L L 2019 Fully coupled modeling of nanosecond pulsed plasma assisted combustion ignition *J. Phys. D: Appl. Phys.* **52** 095204
[13] Tholin F, Lacoste D A and Bourdon A 2014 Influence of fast-heating processes and O atom production by a nanosecond spark discharge on the ignition of a lean-air premixed flame *Combust. Flame* **161** 1235–46
[14] Han J and Yamashita H 2014 Numerical study of the effects of non-equilibrium plasma on the ignition delay of a methane–air mixture using detailed ion chemical kinetics *Combust. Flame* **161** 2064–72
[15] Castela M, Stepanyan S, Fiorina B, Coussement A, Gicquel O, Darabiha N and Laux C O 2017 A 3-D DNS and experimental study of the effect of the recirculating flow pattern inside a reactive kernel produced by nanosecond plasma discharges in a methane-air mixture *Proc. Combust. Inst.* **36** 4095–103
[16] Filimonova E A, Dobrovolskaya A S, Bocharov A N, Bityurin V A and Naidis G V 2020 Formation of combustion wave in lean propane-air mixture with a non-uniform chemical reactivity initiated by nanosecond streamer discharges in the HCCI engine *Combust. Flame* **215** 401–16
[17] Lefkowitz J K, Guo P, Rousso A and Ju Y 2015 Species and temperature measurements of methane oxidation in a nanosecond repetitively pulsed discharge *Phil. Trans. R. Soc.* A **373** 20140333
[18] Pancheshnyi S, Eismann B, Hagelaar G and Pitchford L 2008 *Computer Code ZDPlasKin* (Toulouse: University of Toulouse, LAPLACE: CNRS–UPS–INP)
[19] Kee R J, Rupley F M and Miller J A 1989 *Chemkin-II: A Fortran Chemical Kinetics Package for the Analysis of Gas-phase Chemical Kinetics* (Livermore, CA: Sandia National Labs)
[20] Hagelaar G J M and Pitchford L 2005 Solving the Boltzmann equation to obtain electron transport coefficients and rate coefficients for fluid models *Plasma Sources Sci. Technol.* **14** 722–33
[21] Chen Z, Burke M P and Ju Y 2009 Effects of Lewis number and ignition energy on the determination of laminar flame speed using propagating spherical flames *Proc. Combust. Inst.* **32** 1253–60
[22] Chen Z 2010 Effects of radiation and compression on propagating spherical flames of methane/air mixtures near the lean flammability limit *Combust. Flame* **157** 2267–76
[23] Chen Z, Burke M P and Ju Y 2011 On the critical flame radius and minimum ignition energy for spherical flame initiation *Proc. Combust. Inst.* **33** 1219–26
[24] Chen Z 2015 On the accuracy of laminar flame speeds measured from outwardly propagating spherical flames: methane/air at normal temperature and pressure *Combust. Flame* **162** 2442–53
[25] Wang Y, Han W and Chen Z 2019 Effects of fuel stratification on ignition kernel development and minimum ignition energy of n-decane/air mixtures *Proc. Combust. Inst.* **37** 1623–30
[26] Zhang W, Faqih M, Gou X and Chen Z 2018 Numerical study on the transient evolution of a premixed cool flame *Combust. Flame* **187** 129–36
[27] Faghih M, Li H, Gou X and Chen Z 2019 On laminar premixed flame propagating into autoigniting mixtures under engine-relevant conditions *Proc. Combust. Inst.* **37** 4673–80
[28] Chen Z 2009 Studies on the initiation propagation, and extinction of premixed flames *PhD Thesis* Princeton University
[29] Wang Y, Movaghar A, Wang Z, Liu Z, Sun W, Egolfopoulos F N and Chen Z 2020 Laminar flame speeds of methane/air mixtures at engine conditions: performance of different kinetic models and power-law correlations *Combust. Flame* **218** 101–8
[30] Burke M P, Chaos M, Ju Y, Dryer F L and Klippenstein S J 2012 Comprehensive H_2/O_2 kinetic model for high-pressure combustion *Int. J. Chem. Kinet.* **44** 444–74
[31] Pancheshnyi S, Biagi S, Bordage M C, Hagelaar G, Morgan W L and Phelps A V 2012 The LXCat project: electron scattering cross sections and swarm parameters for low temperature plasma modeling *Chem. Phys.* **398** 148–53
[32] Chen Z and Ju Y 2007 Theoretical analysis of the evolution from ignition kernel to flame ball and planar flame *Combust. Theory Modelling* **11** 427–53
[33] Kelley A P, Jomaas G and Law C K 2009 Critical radius for sustained propagation of spark-ignited spherical flames *Combust. Flame* **156** 1006–13